analytical chemistry

pubs.acs.org/ac Article

Low-Cost Quantitative Photothermal Genetic Detection of Pathogens on a Paper Hybrid Device Using a Thermometer

Wan Zhou, Jianjun Sun, and XiuJun Li*

Cite This: *Anal. Chem.* 2020, 92, 14830−14837 Read Online

ACCESS | Metrics & More | Article Recommendations | Supporting Information

ABSTRACT: Tuberculosis (TB), one of the deadliest infectious diseases, is caused by *Mycobacterium tuberculosis* (*MTB*) and remains a public health problem nowadays. Conventional *MTB* DNA detection methods require sophisticated infrastructure and well-trained personnel, which leads to increasing complexity and high cost for diagnostics and limits their wide accessibility in low-resource settings. To address these issues, we have developed a low-cost photothermal biosensing method for the quantitative genetic detection of pathogens such as *MTB* DNA on a paper hybrid device using a thermometer. First, DNA capture probes were simply immobilized on paper through a one-step surface modification process. After DNA sandwich hybridization, oligonucleotide-functionalized gold nanoparticles (AuNPs) were introduced on paper and then catalyzed the oxidation reaction of 3,3′,5,5′-tetramethylbenzidine (TMB). The produced oxidized TMB, acting as a strong photothermal agent, was used for the photothermal biosensing of *MTB* DNA under 808 nm laser irradiation. Under optimal conditions, the on-chip quantitative detection of the target DNA was readily achieved using an inexpensive thermometer as a signal recorder. This method does not require any expensive analytical instrumentation but can achieve higher sensitivity and there are no color interference issues, compared to conventional colorimetric methods. The method was further validated by detecting genomic DNA with high specificity. To the best of our knowledge, this is the first photothermal biosensing strategy for quantitative nucleic acid analysis on microfluidics using a thermometer, which brings fresh inspirations on the development of simple, low-cost, and miniaturized photothermal diagnostic platforms for quantitative detection of a variety of diseases at the point of care.

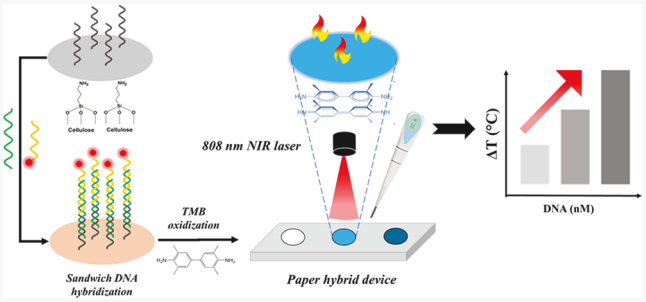

Many pathogens frequently cause global health concerns. Tuberculosis (TB), one of the deadliest infectious diseases, remains a leading cause of death from a single infection across the world.[1,2] High morbidity and mortality of TB pose a significant threat to public health, causing nearly 1.5 million deaths annually.[3] TB is caused by a species of pathogenic bacteria, *Mycobacterium tuberculosis* (*MTB*), which has been traditionally diagnosed via time-consuming clinical examination, sputum smear microscopy, and culture of *MTB* bacteria.[4,5] Recent years have seen a rapid development of laboratory diagnostics for TB based on molecular tests,[3,6] typically *MTB* DNA detection methods, which significantly facilitate early diagnosis of TB, especially for latent infection. Latent TB usually happens at an early stage of infection, where *MTB* is internalized into the phagosomes of host macrophages and exhibits latency.[7−9] However, the latent TB becomes active when *MTB* starts to replicate after rupturing the phagosomal membranes and translocating into the cytosol.[7−9] Researchers have found two types of genes (EsxA and EsxB) and their encoding secreted proteins (6 kDa early secreted antigenic target or ESAT-6 and 10 kDa culture filtrate protein or CFP-10) play an important role in the transition from latent TB to active TB.[7−11] Therefore, these genes can be used as specific targets for *MTB* DNA detection.

To date, various *MTB* DNA detection methods have been developed, including colorimetry,[12,13] electrochemistry,[14,15] fluorescence,[16,17] chemiluminescence,[18,19] etc., which generally rely on the DNA amplification techniques, such as polymerase chain reaction (PCR)[12,20] and loop-mediated isothermal amplification (LAMP).[21,22] For instance, clinical samples were detected quantitatively based on the colorimetric method using PCR-amplified *MTB* DNA, which was based on the target-induced nanoprobe aggregation.[20] However, these detection methods require expensive analytical instruments and professional operators, which have significantly increased the complexity and cost of TB diagnoses and limited their wide accessibility, especially in low-resource settings. Therefore, it is

Received: September 1, 2020
Accepted: October 5, 2020
Published: October 15, 2020

https://dx.doi.org/10.1021/acs.analchem.0c03700
Anal. Chem. 2020, 92, 14830−14837

still challenging and demanding to develop new detection strategies for low cost and quantitative detection of *MTB* DNA.

Recently, nanomaterial-mediated photothermal biosensing methods have emerged as an attractive strategy in the quantitative detection of biomolecules,[23−28] due to the simplicity in the experimental process (such as no need for pneumatic pumps), low cost in data recording (only using a thermometer as a signal reader), and great convenience in analyzing biosensing signals (temperature-based readouts). Several photothermal biosensing platforms have been developed by our research group and other researchers for the detection of biomolecules.[23−26,28−30] By converting the traditional immunosensing signals to photothermal signals (i.e., temperature), biomolecules were quantified by only using a common thermometer. For instance, we developed the first photothermal immunoassay using a common thermometer for quantitative cancer biomarker detection.[23] However, most of the current photothermal biosensing strategies have focused on protein analysis, while photothermal genetic analysis is rarely reported.

Microfluidic lab-on-a-chip (LOC) technology has provided a promising point-of-care (POC) diagnostic tool for various diseases, owing to its miniaturization, portability, low reagent consumption, etc.[31−35] Among numerous LOC devices, paper-based microfluidic devices have attracted much attention given the merits of paper substrates, such as the extremely low cost, ease of manipulation, and three-dimensional (3D) porous microstructures with a high surface-to-volume ratio.[34,36,37] Particularly, by integrating them with other materials, such as rigid polymers, the obtained paper/polymer hybrid microfluidic devices have been capable of meeting assorted requirements for sample immobilization, fluid processing, and signal analyzing, which are suitable for easy and inexpensive nucleic acid analysis at the point of care.[34,38,39] For example, we recently developed a simple, low-cost, and versatile paper-based device for genetic analysis via a one-step surface modification method using 3-aminopropyl trimethoxysilane (APTMS).[36] The nonfunctionalized DNA probes were directly immobilized on paper through ionic interaction between the negatively charged DNA probes and positively charged paper surface. Enhanced DNA immobilization efficiency and detection sensitivity were obtained using the paper substrate. However, this low-cost paper-based microfluidic platform has not been integrated with photothermal biosensing for quantitative DNA detection.

In this study, we have developed a new photothermal biosensing method on a paper hybrid microfluidic device for the low-cost quantitative detection of *MTB* DNA using a thermometer. Target *MTB* DNA (derived from the *MTB* EsxA gene) was recognized via the sandwich hybridization between capture DNA probes and gold nanoparticle (AuNP)-modified detector probes, where the former was simply immobilized on the paper substrate after one-step surface modification. The near-infrared (NIR) photothermal agent, oxidized 3,3′,5,5′-tetramethylbenzidine (ox-TMB),[25] was then produced based on the AuNP-catalyzed TMB oxidization reaction, which further converted target concentration information to temperature readouts under the irradiation of an 808 nm laser. By only using a thermometer, the quantification of target DNA was achieved from the on-chip temperature measurement. As far as we know, this work is the first report to integrate the photothermal biosensing strategy on a paper hybrid microfluidic device for simple, low cost, and quantitative detection of DNA. In comparison with conventional colorimetric methods, this method has provided higher sensitivity with no issues of color interference, while preventing the need for advanced analytical instruments.

EXPERIMENTAL SECTION

Materials and Instruments. Whatman No. 1 chromatography paper, gold nanoparticles (with a diameter of 20 nm), 3,3′,5,5′-tetramethylbenzidine (TMB), Tris(2-carboxyethyl) phosphine hydrochloride (TCEP), (3-aminopropyl) trimethoxysilane (APTMS), bovine serum albumin (BSA), saline-sodium citrate (SSC) buffer (20×, pH 7.0), sodium dodecyl sulfate (SDS), and phosphate-buffered saline (PBS, 10 mM, pH 7.4) were purchased from Sigma (St. Louis, MO). Hydrogen peroxide (H_2O_2, 30% w/w) was purchased from Fisher Scientific (Hampton, NH). Poly(methyl methacrylate) (PMMA, 2.0 mm in thickness) sheets were purchased from Mcmaster-Carr (Los Angeles, CA). All chemicals were used as received without further purification. All buffer solutions were prepared by diluting in PBS buffer, including the washing buffer (2× SSC, 0.1% SDS) and the hybridization buffer (5× SSC, 0.1% SDS, 1% BSA).

All synthetic oligonucleotides were purchased from Integrated DNA Technologies (Coralville, IA) and listed in Table S1. The genomic nucleic acid species were kindly provided by Prof. Jianjun Sun's lab (UTEP), including *M. tuberculosis* (*MTB*), *Mycobacterium smegmatis* (*M. smegmatis*), *Mycobacterium marinum* (*M. marinum*), and *MTB*(ΔEsxAB) (the *MTB* strain with deletion of EsxB:EsxA operon, denoted as TB Knockout herein). The concentrations of the DNA samples were determined via a NanoDrop spectrophotometer (Sigma-Aldrich, St. Louis, MO).

UV−vis characterization was performed on a microplate reader (Molecular Devices, LLC, Sunnyvale, CA). An 808 nm diode laser (Model MDL-III-808, Opto Engine, Midvale, UT) was used to irradiate the samples. The on-chip temperature measurement was obtained using a digital thermometer (e.g., Model 421502, Extech Instruments Corporation). The thermometer has a resolution of 0.1 °C and was used as a signal recorder for the following photothermal biosensing process.

Preparation of DNA Probe−AuNP Conjugates. The DNA probe−AuNP conjugates were prepared freshly modified from a published procedure via the typical salt-aging method.[40,41] First, 3 μL of 100 μM thiolated DNA (SH-DNA) probes was added into a TCEP aqueous solution (6 μL, 100 μM), followed by incubation at room temperature for 30 min. The mixture was then added to 1.0 mL of AuNPs (1.2 nM) and incubated overnight. Aliquots of 120 μL of 1% SDS and 12 μL of 2 M NaCl were added to the suspension slowly, followed by further incubation for 24 h. The obtained suspension was centrifuged at 13 000 rpm for 20 min and washed three times with the washing buffer. The pellet was finally dispersed in PBS buffer (10 mM, pH 7.4, 150 mM NaCl, 0.1% SDS) and stored at 4 °C. The synthesized DNA probe−AuNP conjugates were characterized via UV−vis spectroscopy, and the concentration of AuNPs was determined using the Beer−Lambert law.

Fabrication of the Paper Hybrid Microfluidic Device. The paper/polymer hybrid microfluidic device was designed with the Adobe AI software and fabricated using a chromatography paper and PMMA sheets, following our

https://dx.doi.org/10.1021/acs.analchem.0c03700
Anal. Chem. 2020, 92, 14830−14837

Scheme 1. Working Principle of the AuNP-Mediated Photothermal Biosensing of *MTB* Target DNA on a Paper Hybrid Device Using a Thermometer

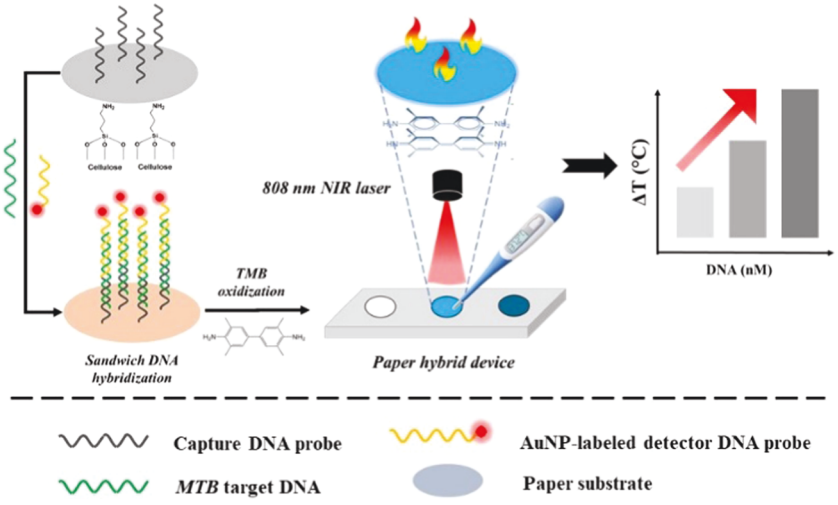

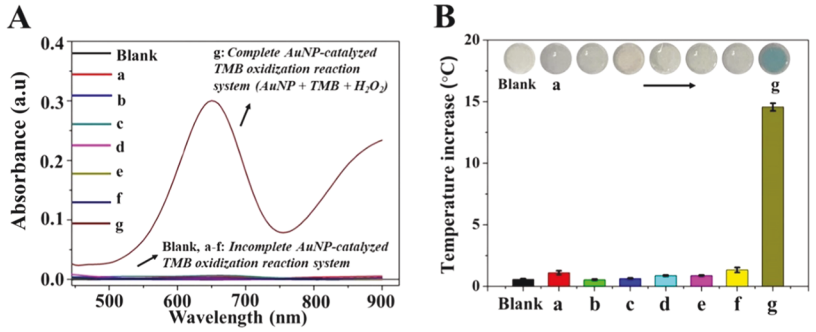

Figure 1. Feasibility tests of the AuNP-mediated photothermal biosensing method. (A) UV−vis spectra and (B) temperature increases of different components in the AuNP-catalyzed TMB oxidization reaction system, including the citrate buffer as blank, (a) TMB, (b) H_2O_2, (c) AuNPs, (d) TMB + H_2O_2, (e) AuNPs + H_2O_2, (f) TMB + AuNPs, and (g) AuNPs + TMB + H_2O_2. The insets are the photographs of the above samples. The laser power density was 0.16 W/mm^2, and the irradiation time was 5 min. The error bars indicate standard deviations (n = 6).

published work.[42−44] Essentially, PMMA sheets were laser-ablated using a laser cutter (Epilog laser, Golden, CO), yielding six reservoirs with a diameter of 3.5 mm and a depth of 1.5 mm for each. The chromatography paper was cut on the laser cutter to form circular regions with a diameter of 3.5 mm and then inserted into PMMA reservoirs. The whole size of the paper/PMMA hybrid device was 75 mm × 18 mm.

On-Chip DNA Hybridization Procedures. To immobilize capture probes on the paper substrate, a surface modification process was adapted based on a reported method from our group.[36] First, 10 μL of 5% APTMS was added to each paper reservoir and incubated for 10 min. After washing thoroughly, the device was dried under ambient temperature. On each APTMS-modified detection zone, 5 μL of 1 μM capture probes was added and incubated for 30 min at 37 °C. A BSA solution (3%, w/v) was then added as the blocking reagent and incubated for 10 min at 37 °C. The DNA probe−AuNP conjugates and target *MTB* DNA with varying concentrations were mixed in a volume ratio of 1:1 and prehybridized for 30 min at 37 °C. The obtained solution was added to the device with 10 μL per reservoir and incubated for 30 min at 37 °C. Notably, washing steps were performed after each incubation step to remove nonspecific binding. Additionally, when using genomic DNA, the samples were first denatured at 95 °C for 5 min and then placed on ice for 1 min before the prehybridization step.

On-Chip Photothermal Biosensing of the Target *MTB* DNA. After DNA hybridization, the substrate mixture containing TMB (0.25 mg/mL), H_2O_2 (1.25 M), and the citrate buffer was added (20 μL per reservoir) and allowed to react for 20 min at room temperature. The 808 nm laser was then used to irradiate each reservoir with a power density of 0.16 W/mm^2. (Note: the irradiation setup was carefully adjusted to achieve comparable sizes between the NIR laser spot and detection reservoirs with a diameter of 3.5 mm.) On-chip temperature measurement was conducted using the thermometer immediately after irradiation. The position of the digital thermometer with a miniaturized probe tip (1.0 mm of diameter) was fixed in all photothermal biosensing processes to avoid temperature variations due to position changes.

RESULTS AND DISCUSSION

Working Principle and Feasibility Tests. The working principle for the photothermal detection of *MTB* DNA on a paper hybrid device is shown in Scheme 1. Essentially, the capture probes are first immobilized on APTMS-modified paper reservoirs (with amine groups) via ionic interaction between the positively charged paper surface and negatively charged DNA probes.[36] When adding target sequences, DNA

https://dx.doi.org/10.1021/acs.analchem.0c03700
Anal. Chem. 2020, 92, 14830−14837

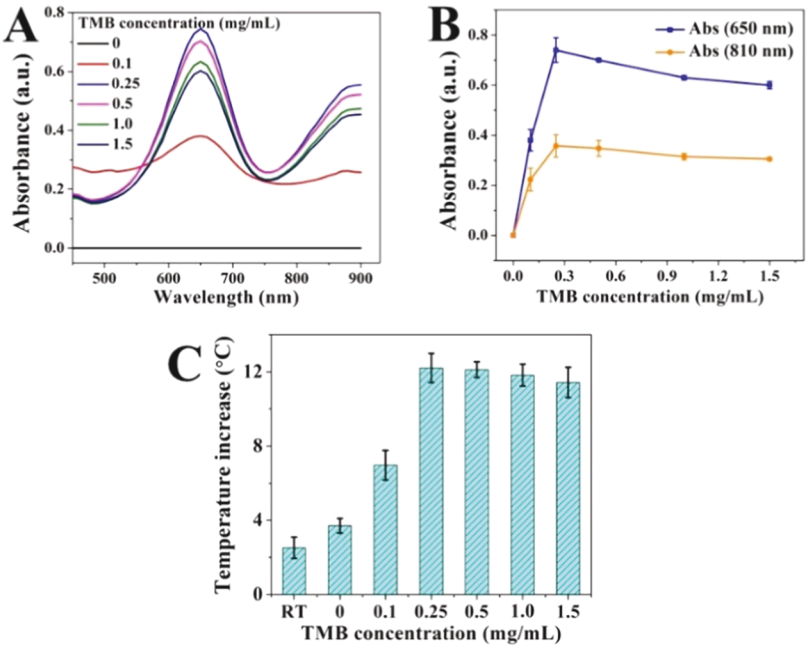

Figure 2. TMB concentration optimization in the AuNP-catalyzed TMB oxidation reaction system. (A) UV−vis spectra, (B) absorbances at 650 and 810 nm, and (C) on-chip temperature measurement of reaction solutions with different TMB concentrations. The laser power density was 0.16 W/mm^2, and the irradiation time was 5 min. The error bars indicate standard deviations (n = 3).

sandwich hybridization occurs among capture probes, target DNA, and AuNP-labeled detector probes. As such, the AuNPs are immobilized on paper. Upon the addition of the substrate TMB, AuNPs catalyze the oxidization reaction of TMB in the presence of H_2O_2 due to the peroxidase-like activity.[45,46] As illustrated in Scheme S1, the ox-TMB is then produced with an obvious color change from colorless to blue via the one-electron charge-transfer process,[47,48] which can be visualized by the naked eye. Importantly, the ox-TMB is a strong NIR photothermal probe from our recent discovery,[25] which is able to efficiently convert photon energy to thermal energy. Under the irradiation of an 808 nm laser, the temperature of reservoirs increases and can be recorded using a thermometer. When increasing concentrations of the target DNA, more AuNPs are captured on paper via DNA hybridization, thereby producing more ox-TMB with darker colors, resulting in a higher temperature increase. Therefore, the temperature signals can be correlated with the target concentrations, and the photothermal biosensing can be achieved for the visual quantitative detection of *MTB* DNA on the paper hybrid device using a thermometer.

The feasibility of the AuNP-mediated photothermal biosensing method was first investigated by testing different components in the system, and the results are shown in Figure 1. Samples (a−g) contained different components in the AuNP-catalyzed TMB oxidization reaction system, including the citrate buffer as blank, (a) TMB, (b) H_2O_2, (c) AuNPs, (d) TMB + H_2O_2, (e) AuNPs + H_2O_2, (f) TMB + AuNPs, and (g) AuNPs + TMB + H_2O_2. All components were added at the same concentrations in all samples, namely, 0.25 mg/mL for TMB as a chromogenic substrate, 1.25 M for H_2O_2 as an oxidizing agent, and 0.03 nM for AuNPs as the catalyst. No obvious differences were observed in the UV−vis spectra and photographs of Samples (a−f) (containing incomplete component combinations in the AuNP-catalyzed TMB oxidization reaction system), whereas an absorption peak at around 650 nm appeared in Sample (g) (containing all components in the AuNP-catalyzed TMB oxidization reaction system) with a clear blue color. It is noted that the characteristic peak of AuNPs (20 nm) at 520 nm is not shown in Sample (c) due to the extremely low concentration (i.e., 0.03 nM), as compared to AuNPs at a higher concentration (i.e., 0.8 nM) in Figure S1, showing a typical peak at 520 nm. The result was consistent with previous studies and confirmed the formation of the oxidized product, ox-TMB, with the characteristic absorption peak.[25] Furthermore, comparing the results from Sample (d) with (g), it was found that the AuNPs were capable of facilitating the oxidization reaction of TMB in the presence of H_2O_2, confirming the peroxidase-mimicking property of AuNPs. Under the irradiation of the 808 nm laser, a significant temperature elevation of nearly 15.0 °C was observed in Sample (g), indicating the strong photothermal conversion efficiency of the ox-TMB, which was attributed to the strong absorption in the NIR region. Contrarily, negligible temperature increases were recorded in other samples. The results showed that temperature changes were only derived from the ox-TMB production, and there was little interference from other components in the on-chip photothermal measurements, confirming the feasibility of the AuNP-mediated photothermal detection method.

Optimization of TMB Concentrations. In this nanomaterial-mediated photothermal biosensing platform, TMB was used as the substrate to produce the photothermal biosensing probe (i.e., ox-TMB), and it is important for the concentration of TMB to be optimized to achieve the best detection performance. The off-chip UV−vis spectroscopy and on-chip temperature measurement were applied to characterize the optimization process. Generally, given a constant concentration of AuNPs (0.8 nM) and the reaction time (20 min), a series of TMB concentrations in the range from 0 to 1.5 mg/mL were tested. As seen in Figure 2A,B, the absorbances at 650

https://dx.doi.org/10.1021/acs.analchem.0c03700
Anal. Chem. 2020, 92, 14830−14837

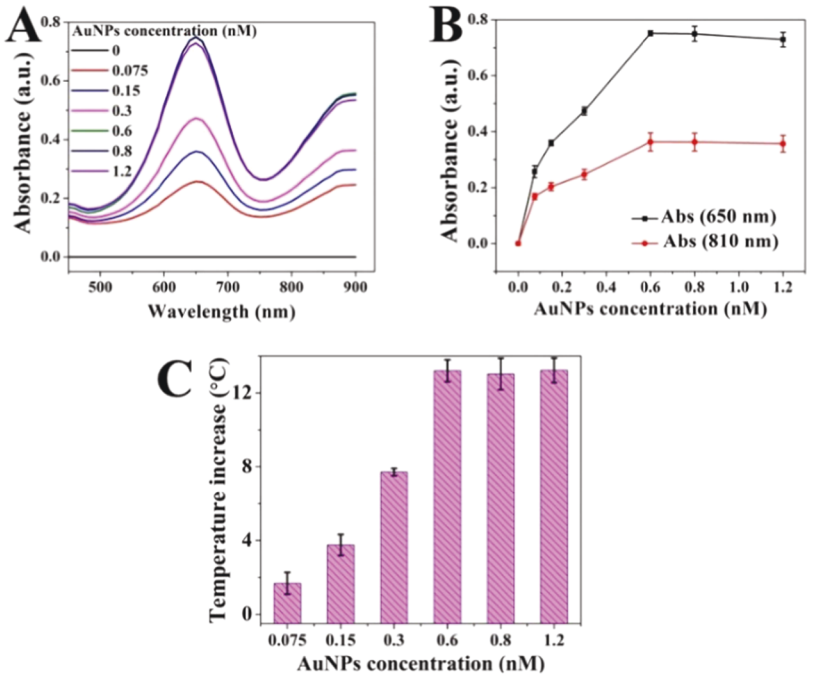

Figure 3. AuNPs concentration optimization in the AuNP-catalyzed TMB oxidization reaction system. (A) UV−vis spectra, (B) absorbances at 650 and 810 nm, and (C) on-chip temperature measurement of reaction solutions with different AuNP concentrations. The laser power density was 0.16 W/mm^2, and the irradiation time was 5 min. The error bars indicate standard deviations (n = 3).

nm (representing the characteristic peak of ox-TMB products) increased in the concentration range of 0−0.25 mg/mL and decreased at higher concentrations. The results indicated that, given a fixed amount of catalysts, the production of ox-TMB was enhanced when increasing substrate concentrations, and it reached the maximum amount when adding 0.25 mg/mL of TMB. When using excessive amounts of TMB, a slight color fading was found, which might be attributed to the formation of a light-yellow colored product because of its further oxidization.[45,49] Similar changes were observed in the absorbances at 810 nm in Figure 2B (representing the typical absorption in the NIR region) with the maximum absorption obtained at 0.25 mg/mL, indicating potential NIR photothermal effects. Under the laser irradiation, the temperature increased sharply from ΔT ~2.0 to 12.0 °C at the TMB concentration from 0 to 0.25 mg/mL and reached a plateau (ΔT ~12.0 °C) afterward, suggesting that the maximum signals were obtained when the concentration of TMB was 0.25 mg/mL (Figure 2C). Therefore, 0.25 mg/mL was used as the optimal TMB concentration in the following tests.

Optimization of AuNPs Concentrations. To obtain the maximum amount of ox-TMB, the concentration of the catalyst (AuNPs) in this TMB oxidization reaction system was also optimized for the best photothermal biosensing performance. By testing different concentrations (0−1.5 nM) of AuNPs, the off-chip UV−vis spectra and on-chip temperature measurement were applied to characterize the optimization process under the optimal concentration (0.25 mg/mL) of TMB. The absorbances at 650 and 810 nm were selected representing the typical peaks of the colorimetric and the NIR photothermal absorption. As shown in Figure 3, the absorbances at 650 nm increased from 0.075 to 0.6 nM, and no obvious change occurred when the concentration was higher than 0.6 nM. Therefore, it can be concluded that the saturated amount of ox-TMB was produced when adding 0.6 nM of AuNPs. Similarly, the absorbances at 810 nm increased in the range of 0.075−0.6 nM and reached a plateau afterward, indicating the maximum NIR absorption at the AuNP concentration of 0.6 nM. Upon laser irradiation, rapid temperature increases were observed when the concentration of AuNPs increased from 0.075 to 0.6 nM. The highest temperature increase with ΔT higher than 12.0 °C was achieved at the AuNP concentration of 0.6 nM, and no significant changes in temperature elevations were recorded in the AuNP concentration range of 0.6−1.2 nM. Consequently, the AuNP concentration was optimized at 0.6 nM and used in the following experiments.

Other Characterizations of the Photothermal Genetic Analysis Platform. In the following AuNP-mediated photothermal biosensing of the target DNA, the DNA probe−AuNP conjugates instead of bare AuNPs were used as the catalyst for the photothermal biosensing probe (ox-TMB). It is worth noting that the DNA probe−AuNP conjugates were synthesized at a constant concentration ratio between the DNA probes and bare AuNPs. The characterization of the conjugates was conducted via UV−vis spectroscopy. As shown in Figure S1, a peak shift from 520 to 530 nm occurred for the conjugates in comparison with bare AuNPs (0.8 nM), which is attributed to the change of surface charges after bioconjugation with oligonucleotides.[50] The concentration of AuNPs in the obtained conjugates was calculated using the Beer−Lambert law based on the extinction coefficient of 8.78 × 108 $M^{-1}\cdot cm^{-1}$,[51,52] and the concentration of conjugated DNA probes was confirmed using the NanoDrop spectrophotometer according to the absorbance at 260 nm. The final molar concentration ratio of the DNA probe−AuNP conjugates was obtained as 220:1 (DNA probes/AuNPs) in our photothermal genetic analysis platform.

To characterize the effect of the irradiation time and obtain the maximum temperature signals, kinetic studies were

https://dx.doi.org/10.1021/acs.analchem.0c03700
Anal. Chem. 2020, 92, 14830−14837

conducted for the photothermal biosensing of the target DNA. Under continuous laser irradiation, the dynamic temperature changes of both the control (in the absence of target DNA) and a sample (in the presence of 10 μM target DNA) were monitored for 6 min. The results are shown in Figure 4A, and

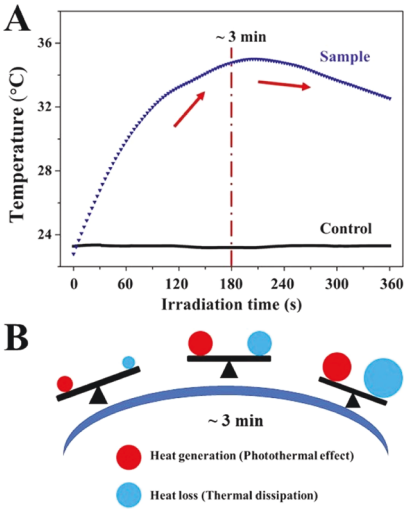

Figure 4. Kinetic studies in the photothermal biosensing process. (A) Dynamic temperature measurement of the control (containing 0 μM target DNA) and the sample (containing 10 μM target DNA) under continuous laser irradiation. The laser power density was 0.16 W/mm^2. (B) Schematic illustration of competitive effects between heat generation and heat loss during the photothermal biosensing process.

the effects of different factors on the photothermal measurement are illustrated in Figure 4B. There was no obvious temperature increase found in the control as compared to room temperature (~23.0 °C). In the presence of the target DNA, a rapid temperature increase was observed from 23.0 to 33.0 °C in the first 120 s due to the strong photothermal conversion. From 120 to 180 s, the temperature of the sample increased slowly, which might be due to enhanced heat loss resulted from a greater temperature gradient between the sample and the surroundings, as a higher sample temperature was achieved than before. At around 3 min, the temperature reached the highest value of ~35.0 °C, suggesting the balance between heat generation (due to the photothermal effect of ox-TMB) and heat loss (due to thermal dissipation). After 3 min, the temperature began gradually decreasing, possibly because photothermal conversion became saturated and heat loss became the predominant factor. Therefore, to achieve the sensitive photothermal biosensing of the target DNA, the laser irradiation time of 3 min was used in the following experiments.

On-Chip Visual Photothermal Detection of *MTB* DNA Using a Thermometer. Under optimal conditions, the on-chip photothermal detection of *MTB* DNA was performed by recording temperature increases of the samples using a thermometer. A series of different concentrations in the range of 0−50 μM for the synthetic *MTB* DNA samples were tested. As shown in the images in Figure 5 insets (a and b), blue color was clearly observed when testing the target DNA (such as at the concentration of 50 μM), while no color change was found in the absence of the target DNA (0 μM). In the photothermal biosensing results, the temperature of the samples increased when adding higher concentrations of the

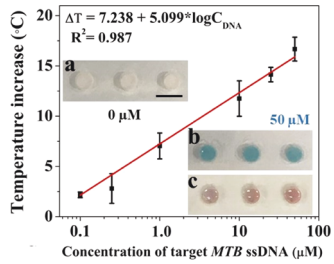

Figure 5. Quantitative photothermal biosensing of *MTB* DNA on the paper hybrid microfluidic device using a thermometer. The calibration curve of temperature increase was plotted versus the logarithmic concentration of target *MTB* ssDNA in the range of 0.1−50 μM. The insets are the photographs of the biosensing samples at the target concentrations of (a) 0 μM, (b) 50 μM, and (c) 50 μM using blood-mimicking dye solutions (scale bar: 5 mm). The laser power density was 0.16 W/mm^2, and the irradiation time was 3 min. The error bars indicate standard deviations (n = 6).

target and reached a ΔT value of nearly 17.0 °C at 50 μM of the target DNA. The plot in Figure 5 shows a linear relationship between temperature increases and the logarithmic concentrations of the synthetic target DNA in the range of 100 nM to 50 μM. The square of the correlation coefficient was 0.987, with a slope of 5.099 °C·μM^{-1}. The limit of detection (LOD) was calculated to be 39 nM (or 0.58 μg/mL) based on the 3-fold standard deviation over the blank.

It is noted that in comparison with the conventional colorimetric biosensing methods,[53−55] there are several significant advantages in our photothermal detection method. First, the proposed method provides higher sensitivity for the detection of the target DNA, obtaining a lower LOD value (0.58 μg/mL) than those reported based on colorimetric signals (LODs: 10,[53] 1.88,[54] or 1.14 μg/mL[55]). In addition, with only a simple and inexpensive signal reader (a thermometer), quantitative detection of DNA can be achieved, avoiding the need for bulky and expensive instruments (such as spectrometers) and significantly reducing the bioassay cost. Furthermore, the quantification of DNA is based on temperature readouts, thereby avoiding color interference from the sample matrix, which is usually a common problem in colorimetric biosensing methods in testing the colored real samples, such as blood matrices. Herein, we used a food dye (red color) to mimic the real colored matrix of a blood sample, and the observation of the blue-colored ox-TMB products was interfered remarkably due to the red color background. The inset (c) in Figure 5 shows a pink color, instead of a blue color from the inset (b) when testing the colorless samples. We did not see such an interference problem in our thermometer-based method, which is another advantage of our method over the colorimetric method.

Specificity Tests. The on-chip photothermal biosensing method was further validated by investigating the specificity for the detection of genomic DNA instead of synthetic sequences. In addition to *MTB* genomic DNA, other interfering species were used, including water as blank, PBS buffer, TB knockout DNA (with the deletion of EsxB:EsxA from *MTB*), *M. smegmatis* (a nonpathogenic mycobacterium that has been widely used as an alternative for *MTB* due to the fast growth and the requirement of low biosafety level facility[56]), a DNA mixture from the above species (*M. smegmatis* and TB knockout), and *M. marinum* (a pathogenic nontuberculous mycobacterium).[57] As shown in Figure 6, a significant

https://dx.doi.org/10.1021/acs.analchem.0c03700
Anal. Chem. 2020, 92, 14830−14837

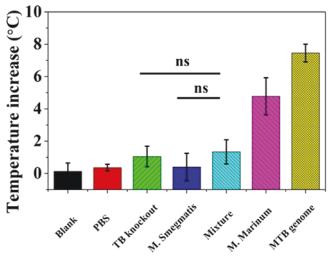

Figure 6. Specificity tests of the photothermal biosensing of genomic *MTB* DNA on the paper hybrid microfluidic device using a thermometer. Temperature increases of the samples containing water as blank, PBS buffer, TB knockout DNA (50 μg/mL), *M. smegmatis* DNA (50 μg/mL), mixture species (*M. smegmatis* and TB knockout, at a final DNA concentration of 50 μg/mL), *M. marinum* DNA (50 μg/mL), and genomic *MTB* DNA (25 μg/mL). The laser power density was 0.16 W/mm^2, and the irradiation time was 3 min. The error bars indicate standard deviations (n = 6). (Statistical significance was calculated using Student's t-test; ns indicates not significant between the two groups, $p > 0.05$).

temperature increase of approximately 8.0 °C was acquired in the detection of *MTB* genomic DNA with the analytical recovery of 113 ± 1%, even at a 2-fold lower concentration than others, while neglectable temperature increases were obtained from blank, PBS buffer, TB knockout DNA, and *M. smegmatis* DNA. Even when testing a mixture of the DNA interference samples containing *M. smegmatis* and TB knockout, the photothermal biosensing signals remained similar to those from individual components, indicating the high specificity of our method. It was noted that the sample containing *M. marinum* genomic DNA at 2-fold higher concentrations had a mild temperature increase of 5.0 °C, which was mainly due to a high percent identity (over 80%) in the genomes between *MTB* and *M. marinum*.[58,59] Therefore, it can be concluded that the proposed photothermal biosensing method has high specificity even when distinguishing the interfering substances with high similarity.

CONCLUSIONS

In conclusion, we have developed a low-cost photothermal biosensing method for visual quantitative nucleic acid detection on a paper hybrid device using a thermometer. By applying the AuNP-mediated photothermal effect in bioassays, the target DNA was quantitatively detected using temperature signals as analytical readouts, achieving higher sensitivity with no color interference, contrasting that from conventional colorimetric detection methods. The entire assay for the quantitative detection of *MTB* DNA as a model target can be completed within 2 h on a low-cost paper/polymer hybrid device (the material cost of $0.08 for each device), without the need for any costly instrumentation and complicated nucleic acid amplification procedures. This method was further validated by detecting genomic DNA with high specificity. To the best of our knowledge, this is the first attempt to perform photothermal genetic analysis on paper hybrid microfluidic devices, providing a simple, low-cost, rapid, and quantitative photothermal microfluidic biosensing platform. With the rapid development of commercially available portable lasers, the portability of this photothermal platform will be further enhanced.

Since this photothermal genetic biosensing platform is based on nucleic acid hybridization, it may find a good niche in a wide range of biological applications based on conventional DNA hybridization techniques such as DNA microarray. Although the DNA microarray technique can provide high throughput, it usually requires costly fluorescence scanners. The proposed assay outperforms conventional DNA microarray (e.g., using glass slides as substrates) in genetic analysis in terms of the aspects of simplicity, ease of operation, affordability, etc. The combination of all of these significant features with a low-cost and portable paper hybrid microfluidic device makes it particularly suitable for POC applications. Many new complementary genetic assays using a thermometer as the signal reader are expected to be developed in the near future. Overall, considering genetic analysis is widely used in various biological applications including infectious disease diagnosis, this photothermal biosensing platform has great potential for broad applications, such as POC disease diagnosis, especially in resource-poor settings.

ASSOCIATED CONTENT

Supporting Information

The Supporting Information is available free of charge at https://pubs.acs.org/doi/10.1021/acs.analchem.0c03700.

Additional schematic illustration of TMB oxidation reaction, DNA sequences, UV−vis spectra of AuNPs, and DNA−AuNP conjugates (PDF)

AUTHOR INFORMATION

Corresponding Author

XiuJun Li − *Department of Chemistry and Biochemistry, Biomedical Engineering, Border Biomedical Research Center, and Environmental Science and Engineering, University of Texas at El Paso, El Paso, Texas 79968, United States;* orcid.org/0000-0002-7954-0717; Email: xli4@utep.edu

Authors

Wan Zhou − *Department of Chemistry and Biochemistry, University of Texas at El Paso, El Paso, Texas 79968, United States;* orcid.org/0000-0002-1439-9548

Jianjun Sun − *Department of Biological Sciences, University of Texas at El Paso, El Paso, Texas 79968, United States;* orcid.org/0000-0001-9399-7644

Complete contact information is available at: https://pubs.acs.org/10.1021/acs.analchem.0c03700

Notes

The authors declare the following competing financial interest(s): XL and WZ submitted a patent application.

ACKNOWLEDGMENTS

We would like to acknowledge the financial support to our current research from the National Institute of Allergy and Infectious Disease of the NIH (R21AI107415), the U.S. NSF (IIP 1953841), the University of Texas at El Paso (UTEP) for the IDR Program, the Philadelphia Foundation, and the Medical Center of the Americas Foundation. Previous financial support to our research from the National Institute of General Medical Sciences of the NIH (SC2GM105584), the NIH RCMI Pilot Grant, the U.S. NSF (DMR1827745 and DMR1205302), the University of Texas (UT) System for the STARS award, and the Multidisciplinary Research Award Program (MRAP), and the URI Program from UTEP is also

greatly acknowledged. We also thank the Dr. Keelung Hong Research Fellowship for the support to W.Z.

REFERENCES

(1) Andersen, P.; Munk, M. E.; Pollock, J. M.; Doherty, T. M. *Lancet* **2000**, *356*, 1099−1104.
(2) Storla, D. G.; Yimer, S.; Bjune, G. A. *BMC Public Health* **2008**, *8*, No. 15.
(3) World Health Organization. *Global Tuberculosis Report 2019*; World Health Organization: Geneva, 2019.
(4) Cheon, S. A.; Cho, H. H.; Kim, J.; Lee, J.; Kim, H. J.; Park, T. J. *J. Microbiol. Methods* **2016**, *123*, 51−61.
(5) Goletti, D.; Petruccioli, E.; Joosten, S. A.; Ottenhoff, T. H. *Infect. Dis. Rep.* **2016**, *8*, No. 6568.
(6) Boehme, C. C.; Nabeta, P.; Hillemann, D.; Nicol, M. P.; Shenai, S.; Krapp, F.; Allen, J.; Tahirli, R.; Blakemore, R.; Rustomjee, R.; Milovic, A.; Jones, M.; O'Brien, S. M.; Persing, D. H.; Ruesch-Gerdes, S.; Gotuzzo, E.; Rodrigues, C.; Alland, D.; Perkins, M. D. *N. Engl. J. Med.* **2010**, *363*, 1005−1015.
(7) De Leon, J.; Jiang, G.; Ma, Y.; Rubin, E.; Fortune, S.; Sun, J. *J. Biol. Chem.* **2012**, *287*, 44184−44191.
(8) Peng, X.; Jiang, G.; Liu, W.; Zhang, Q.; Qian, W.; Sun, J. *FEBS Lett.* **2016**, *590*, 509−519.
(9) Peng, X.; Sun, J. *Toxicon* **2016**, *116*, 29−34.
(10) van der Wel, N.; Hava, D.; Houben, D.; Fluitsma, D.; van Zon, M.; Pierson, J.; Brenner, M.; Peters, P. J. *Cell* **2007**, *129*, 1287−1298.
(11) Simeone, R.; Sayes, F.; Song, O.; Groschel, M. I.; Brodin, P.; Brosch, R.; Majlessi, L. *PLoS Pathog.* **2015**, *11*, No. e1004650.
(12) Hundie, G. B.; Woldemeskel, D.; Gessesse, A. *PLoS One* **2016**, *11*, No. e0169188.
(13) Veigas, B.; Fortunato, E.; Baptista, P. V. *Methods Mol. Biol.* **2015**, *1256*, 41−56.
(14) Ng, B. Y. C.; Wee, E. J. H.; West, N. P.; Trau, M. *ACS Sens.* **2016**, *1*, 173−178.
(15) Tsaloglou, M. N.; Nemiroski, A.; Camci-Unal, G.; Christodouleas, D. C.; Murray, L. P.; Connelly, J. T.; Whitesides, G. M. *Anal. Biochem.* **2018**, *543*, 116−121.
(16) Kamariza, M.; Shieh, P.; Ealand, C. S.; Peters, J. S.; Chu, B.; Rodriguez-Rivera, F. P.; Sait, M. R. B.; Treuren, W. V.; Martinson, N.; Kalscheuer, R.; Kana, B. D.; Bertozzi, C. R. *Sci. Transl. Med.* **2018**, *10*, No. eaam6310.
(17) Tang, N.; Frank, A.; Pahalawatta, V.; Lampinen, J.; Coblenz-Korte, A.; Dunn, C.; Li, C.; Cloherty, G.; Abravaya, K.; Leckie, G. *Tuberculosis* **2015**, *95*, 613−619.
(18) He, Y.; Liu, D. Q.; He, X. Y.; Cui, H. *Chem. Commun.* **2011**, *47*, 10692−10694.
(19) He, Y.; Huang, G. M.; Cui, H. *ACS Appl. Mater. Interfaces* **2013**, *5*, 11336−11340.
(20) Tsai, T. T.; Huang, C. Y.; Chen, C. A.; Shen, S. W.; Wang, M. C.; Cheng, C. M.; Chen, C. F. *ACS Sens.* **2017**, *2*, 1345−1354.
(21) Yee, E. H.; Sikes, H. D. *ACS Sens.* **2020**, *5*, 308−312.
(22) Rafati, A.; Gill, P. *Microchim. Acta* **2015**, *182*, 523−530.
(23) Fu, G. L.; Sanjay, S. T.; Dou, M. W.; Li, X. J. *Nanoscale* **2016**, *8*, 5422−5427.
(24) Fu, G. L.; Sanjay, S. T.; Li, X. J. *Analyst* **2016**, *141*, 3883−3889.
(25) Fu, G. L.; Sanjay, S. T.; Zhou, W.; Brekken, R. A.; Kirken, R. A.; Li, X. J. *Anal. Chem.* **2018**, *90*, 5930−5937.
(26) Zhou, W.; Hu, K. Q.; Kwee, S.; Tang, L.; Wang, Z. H.; Xia, J. F.; Li, X. J. *Anal. Chem.* **2020**, *92*, 2739−2747.
(27) Du, S. Y.; Wang, Y.; Liu, Z. C.; Xu, Z. X.; Zhang, H. Y. *Biosens. Bioelectron.* **2019**, *144*, No. 111670.
(28) Han, X.; Lin, S.; Li, Y.; Cheng, C.; Han, X. *Anal. Chim. Acta* **2020**, *1098*, 117−124.
(29) Li, X.; Yang, L.; Men, C.; Xie, Y. F.; Liu, J. J.; Zou, H. Y.; Li, Y. F.; Zhan, L.; Huang, C. Z. *Anal. Chem.* **2019**, *91*, 4444−4450.
(30) Wei, Y.; Wang, D.; Zhang, Y.; Sui, J.; Xu, Z. *Biosens. Bioelectron.* **2019**, *140*, No. 111345.
(31) Sanjay, S. T.; Zhou, W.; Dou, M. W.; Tavakoli, H.; Ma, L.; Xu, F.; Li, X. J. *Adv. Drug Delivery Rev.* **2018**, *128*, 3−28.
(32) Fu, G.; Zhou, W.; Li, X. *Lab Chip* **2020**, *20*, 2218−2227.
(33) Tavakoli, H.; Zhou, W.; Ma, L.; Perez, S.; Ibarra, A.; Xu, F.; Zhan, S.; Li, X. *TrAC, Trends Anal. Chem.* **2019**, *117*, 13−26.
(34) Dou, M.; Macias, N.; Shen, F.; Bard, J. D.; Dominguez, D. C.; Li, X. *EClinicalMedicine* **2019**, *8*, 72−77.
(35) Wei, X. F.; Zhou, W.; Sanjay, S. T.; Zhang, J.; Jin, Q. J.; Xu, F.; Dominguez, D. C.; Li, X. J. *Anal. Chem.* **2018**, *90*, 9888−9896.
(36) Zhou, W.; Feng, M.; Valadez, A.; Li, X. *Anal. Chem.* **2020**, *92*, 7045−7053.
(37) Xu, X. Y.; Wang, X. M.; Hu, J.; Gong, Y.; Wang, L.; Zhou, W.; Li, X. J.; Xu, F. *Electrophoresis* **2019**, *40*, 914−921.
(38) Tavakoli, H.; Zhou, W.; Ma, L.; Guo, Q.; Li, X. *Nanotechnol. Microfluid.* **2020**, 177−209.
(39) Dou, M.; Sanjay, S. T.; Dominguez, D. C.; Liu, P.; Xu, F.; Li, X. *Biosens. Bioelectron.* **2017**, *87*, 865−873.
(40) Thiruppathiraja, C.; Kamatchiammal, S.; Adaikkappan, P.; Santhosh, D. J.; Alagar, M. *Anal. Biochem.* **2011**, *417*, 73−79.
(41) Xu, S. M.; Yuan, H.; Xu, A.; Wang, J.; Wu, L. J. *Langmuir* **2011**, *27*, 13629−13634.
(42) Sanjay, S. T.; Li, M.; Zhou, W.; Li, X.; Li, X. *Microsyst. Nanoeng.* **2020**, *6*, No. 28.
(43) Dou, M. W.; Sanjay, S. T.; Dominguez, D. C.; Zhan, S. H.; Li, X. J. *Chem. Commun.* **2017**, *53*, 10886−10889.
(44) Sanjay, S. T.; Dou, M.; Sun, J.; Li, X. *Sci. Rep.* **2016**, *6*, No. 30474.
(45) Stefan, L.; Denat, F.; Monchaud, D. *Nucleic Acids Res.* **2012**, *40*, 8759−8772.
(46) Fu, G.; Sanjay, S. T.; Zhou, W.; Brekken, R. A.; Kirken, R. A.; Li, X. *Anal. Chem.* **2018**, *90*, 5930−5937.
(47) Shah, J.; Purohit, R.; Singh, R.; Karakoti, A. S.; Singh, S. *J. Colloid Interface Sci.* **2015**, *456*, 100−107.
(48) Huang, L.; Cao, Y. J.; Sun, X. Y.; Liu, B.; Shen, J. S. *Org. Biomol. Chem.* **2018**, *16*, 5667−5676.
(49) Wang, S.; Chen, W.; Liu, A. L.; Hong, L.; Deng, H. H.; Lin, X. H. *ChemPhysChem* **2012**, *13*, 1199−1204.
(50) Li, F.; Zhang, H. Q.; Dever, B.; Li, X. F.; Le, X. C. *Bioconjugate Chem.* **2013**, *24*, 1790−1797.
(51) Zuber, A.; Purdey, M.; Schartner, E.; Forbes, C.; van der Hoek, B.; Giles, D.; Abell, A.; Monro, T.; Ebendorff-Heidepriem, H. *Sens. Actuators, B* **2016**, *227*, 117−127.
(52) Liu, X. O.; Atwater, M.; Wang, J. H.; Huo, Q. *Colloids Surf., B* **2007**, *58*, 3−7.
(53) Veigas, B.; Jacob, J. M.; Costa, M. N.; Santos, D. S.; Viveiros, M.; Inacio, J.; Martins, R.; Barquinha, P.; Fortunato, E.; Baptista, P. V. *Lab Chip* **2012**, *12*, 4802−4808.
(54) Liandris, E.; Gazouli, M.; Andreadou, M.; Comor, M.; Abazovic, N.; Sechi, L. A.; Ikonomopoulos, J. *J. Microbiol. Methods* **2009**, *78*, 260−264.
(55) Bakthavathsalam, P.; Rajendran, V. K.; Mohammed, J. A. B. *J. Nanobiotechnol.* **2012**, *10*, No. 8.
(56) Martini, M. C.; Zhou, Y.; Sung, H. M.; Shell, S. S. *Front. Microbiol.* **2019**, *10*, No. 591.
(57) Sette, C. S.; Wachholz, P. A.; Masuda, P. Y.; Figueira, R. B. F. D.; Mattar, F. R. D.; Ura, D. G. *J. Venomous Anim. Toxins Incl. Trop. Dis.* **2015**, *21*, No. 7.
(58) Tobin, D. M.; Ramakrishnan, L. *Cell. Microbiol.* **2008**, *10*, 1027−1039.
(59) Stinear, T. P.; Seemann, T.; Harrison, P. F.; Jenkin, G. A.; Davies, J. K.; Johnson, P. D. R.; Abdellah, Z.; Arrowsmith, C.; Chillingworth, T.; Churcher, C.; Clarke, K.; Cronin, A.; Davis, P.; Goodhead, I.; Holroyd, N.; Jagels, K.; Lord, A.; Moule, S.; Mungall, K.; Norbertczak, H.; Quail, M. A.; Rabbinowitsch, E.; Walker, D.; White, B.; Whitehead, S.; Small, P. L. C.; Brosch, R.; Ramakrishnan, L.; Fischbach, M. A.; Parkhill, J.; Cole, S. T. *Genome Res.* **2008**, *18*, 729−741.

https://dx.doi.org/10.1021/acs.analchem.0c03700
Anal. Chem. 2020, 92, 14830−14837

Supporting Information

Low-Cost Quantitative Photothermal Genetic Detection of Pathogens on a Paper Hybrid Device Using a Thermometer

Wan Zhou,[†] Jianjun Sun,[§] and XiuJun Li*[,†,#,⊥]

[†]*Department of Chemistry and Biochemistry, University of Texas at El Paso, 500 West University Ave, El Paso, Texas, 79968, USA*

[§]*Department of Biological Sciences, University of Texas at El Paso, 500 West University Ave, El Paso, Texas, 79968, USA*

[#]*Biomedical Engineering, Border Biomedical Research Center, University of Texas at El Paso, 500 West University Ave, El Paso, Texas, 79968, USA*

[⊥] *Environmental Science and Engineering, the University of Texas at El Paso, 500 West University Ave, El Paso, Texas, 79968, USA*

*Corresponding author E-mail: xli4@utep.edu

Table of Contents

Scheme S1. Schematic illustration of the AuNP-catalyzed TMB oxidization reaction.

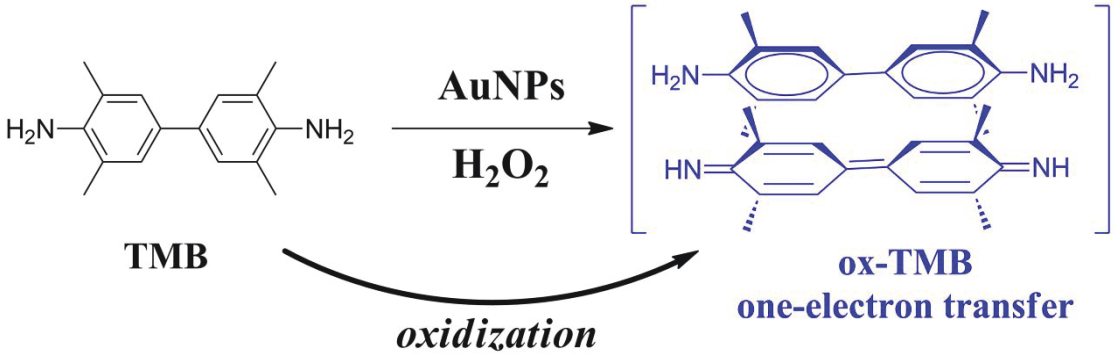

Table S1. DNA sequences used in the photothermal detection method.

DNA	**Sequences (5'-3')**
Capture probe	ATA AAG TTG GTG TTC TGC CCG TTC
Detector probe	TTC ACG TGC GAC ACG ATA GGC GCC $(A)_{15}$ SH
Synthetic target *MTB*	GGC GCC TAT CGT GTC GCA CGT GAA GAA CGG
DNA (EsxA genes)	GCA GAA CAC CAA CTT TAT

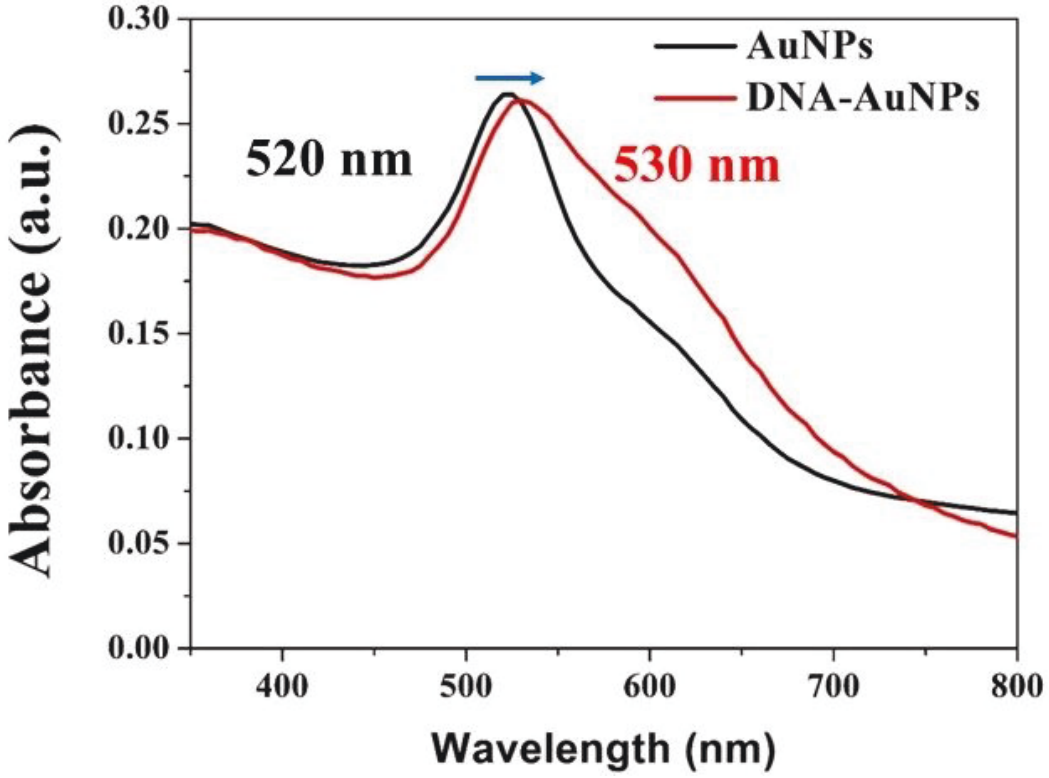

Figure S1. UV-vis spectra of the bare AuNPs and the as-produced DNA probe-AuNP conjugates.